Modeling and simulation of the probe tip based nanochannel scratching

Z. Guo[1], Y. Tian*[1,2], X. Liu[2], F. Wang[1], C. Zhou[1], D. Zhang[1]

[1]Key Laboratory of Mechanism Theory and Equipment Design of Ministry of Education, Tianjin University,

Tianjin 300072, China

[2]School of Engineering, University of Warwick, Coventry CV4 7AL, UK

Abstract

This paper presents the theoretical modeling and numerical simulation of the probe tip based nanochannel scratching. According to the scratching depth, the probe tip is modeled as a spherical capped conical tip or a spherical capped regular three side pyramid tip to calculate the normal force needed for the nanochannel scratching. In order to further investigate the impact of scratching speed, scratching depth and scratching direction on the scratching process, the scratching simulation is implemented in LS-DYNA software, and a mesh-less method called smooth particle hydrodynamics (SPH) is used for the sample construction. Based on the theoretical and simulated analyses, the increase of the scratching speed, the scratching depth and the face angle will result in an increase in the normal force. At the same scratching depth, the normal forces of the spherical capped regular three side pyramid tip model are different in different scratching directions, which are in agreement with the theoretical calculations in the d_3 and d_4 directions. Moreover, the errors between the theoretical and simulated normal forces increase as the face angle increases.

Key words: tip modeling; nanochannel scratching; SPH; normal force.

1. Introduction

Nanochannels have wide applications in microfluidics technology, such as rapid DNA sequencing, drug delivery, battery and nanofluidic transistor [1]. Among various methods of nanochannel fabrication, probe tip based micro/nano scratching has been widely applied [2-6]. In the nanochannel scratching, the sample is usually mounted on a piezoelectric actuated micro/nano positioning stage, which has many excellent advantages including fast response time, large mechanical force and high positioning precision, there have been many investigations on the modeling and control of this kind of stage [7]. As the cutting tool, the probe tip is pressed into the sample with a desired depth, and then through the motion control of the precision positioning stage, the nanochannel can be fabricated on the sample surface.

Various kinds of probe tip models have been developed in the past few years. According to the tip geometry, they can be mainly categorized into spherical tips [8-10], conical tips [11, 12] and pyramidal tips [13-15]. The spherical tip is usually with a diameter in the micron scale, which is not appropriate for the nanochannel fabrication. For the conical tip and pyramidal tip, it is impossible to obtain an ideal sharp tip due to manufacturing errors and tip wear, thus, these tips are usually modeled as a conical or pyramidal base with spherical cap. If only the spherical cap is involved in the operation for the surface topography measurement and scratching, the tip is still modeled as a sphere. However, in the scratching with large depth, the tip base will dominate the scratching process, so the tip base must be considered in such kind of application. Although the spherical capped conical model has been widely used, but it cannot substitute the pyramid structure. Geng proposed the spherical capped pyramidal tip model for the AFM tip, and the tip-sample interface was analyzed for single scratching [13], but the calculation of the horizontal projected area is complicated. Besides the AFM probe tip, the Berkovich probe has also been used for scratching investigation, but the scratching direction was not be considered [14-16], this kind of tip has regular pyramidal structure, which has many special geometry property compared with the general pyramidal structure, such as equilateral triangle of horizontal cross-section.

As a supplementary means for theoretical analysis, the numerical simulation usually acts as the role of guiding the experiments, and shows the possible phenomenon in the actual experiment. Molecular dynamics (MD) is an efficient method for the investigation of the micro/nano scratching, and which has been adopted by many researchers. Zhu et al investigated the effect of the scratching velocity on the scratching process in reference [17-19]. Zhang explored the subsurface deformed layers in AFM-based nanometric cutting process through molecular dynamics simulation [20]. Yan studied the effect of feed on the nano-scratching process using MD simulation [21]. Zhang examined the influence of double-tip scratch on nano scratching process via MD [22]. Fang researched the nanoscratch behavior of multi-layered films with MD [23]. However, in all these simulations, the scratching depth was less than 10 nanometers, since a larger scratching depth will result in a very long simulation time. Thus, MD is not an appropriate method for the simulation of dozens even hundreds nanometer scratching depth.

Smooth particle hydrodynamic (SPH) is a mesh-less method based on Lagrangian method, which is firstly proposed by Gingold and Monaghan in 1977 to solve the astrophysical problems [24], but with the development of the method, it has been widely used in fluid simulation and solid mechanics for the advantages in dealing with the large distortions [25, 26]. Furthermore, the method has been successfully applied in micro machining simulation in

recent years [27-29]. Zhao studied the effects of cutting process on residual stress distribution, and the effects of residual stress on mechanism using SPH method [27], the cutting depth is from 300nm to 900nm. And then still with SPH method, his team further investigated the residual stress on sequential scratching with smaller scratching depth from 50nm to 150nm [28]. Cao compared the conventional scratching with the ultrasonic-assisted scratching on the material removal process, two scratching depth 70nm and 2μm were simulated with SPH [29].

In the tip based nanochannel scratching, the normal force is an important parameter because it directly decides the scratching depth, so this paper focuses on the theoretical calculation and the simulation of the normal force. Among various probe tips, the three side pyramid probe tip is the most popular for the good machining ability, thus a spherical capped regular three side pyramidal tip model is chosen to model this kind of tips in large scratching depth. The geometrical model of the spherical capped conical tip and the spherical capped regular three side pyramidal tip are firstly introduced in this paper, and then the horizontal projected areas of the tip-sample interfaces are analyzed in section 2. The SPH simulation model are constructed in section 3, the effects of the scratching parameters (scratching speed, scratching depth and scratching direction) and the face angle of the probe tip on the scratching process are simulated and discussed in section 4.

2. The probe tip model and the horizontal projected area of the tip-sample interface

In this section, two probe tip models are presented, one is spherical capped conical tip model and the other is spherical capped regular three side pyramidal tip model. The scratching depth considered in this paper is from 20nm to 200nm, and the spherical cap radius is assumed to be 90 nm. When the scratching depth is less than 60nm, only the spherical cap takes part in the scratching, the former tip model has a complete spherical surface in this range, so it is selected for the simulation in this scratching range. When the scratching depth is larger than 60nm, the probe base will dominate the scratching, the latter tip model is more similar with the actual three side pyramid probe tip in geometric features, so it is selected for the simulation in this range of scratching depth.
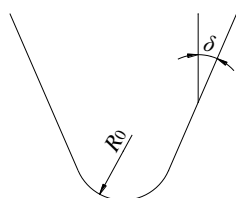

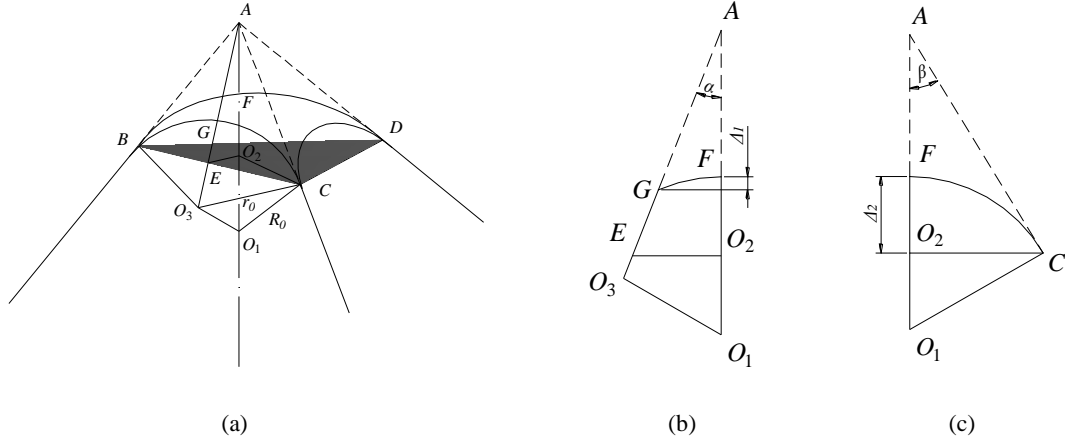Fig. 1. Spherical capped conical tip model

Fig. 2. (a) Spherical capped regular three side pyramidal tip model; (b) Section of the triangle ΔAO_1O_3; (c) Section of the triangle ΔAO_1C.

2.1 Geometrical model

A spherical capped conical tip model has been widely applied in the analysis of the tip-sample interface [10, 11], which is shown in Fig. 1, where R_0 is the spherical cap radius and δ is the half angle. In precious paper, both the spherical cap and the conical base are used for the scratching, but in this paper only the spherical cap is selected for the small scratching depth under 60nm, the cone part is seen as the assumptive probe tip base, so the value of δ does not affect the scratching process and the tip-sample interface.

For the large scratching depth from 60nm to 200nm, a spherical capped regular three side pyramidal tip model is presented, as shown in Fig. 2(a). The point A is the hypothetical apex, and the triangle ΔBCD is the critical horizontal section interface between spherical cap and pyramid base. The arcs BC, CD and BD are the intersection of spherical surface and pyramidal surfaces, which are assumed to be tangent to the pyramidal edges. Figs. 2(b) and (c) are the section of triangle ΔAO_1O_3 and ΔAO_1C, respectively, where O_1 is the center of spherical cap surface with a radius R_0, O_3 is the center of arc BC with a radius r_0. In order to facilitate the scratching analysis, three angles α, β and γ are defined as face angle, edge angle and side angle, respectively, the side angle is also the groove angle when scratching in the directions of d_1 and d_2. For a regular three side pyramidal probe tip, the spherical cap radius R_0 and the face angle α can be obtained through the measurement. Compared with the general three side pyramid, the regular three side pyramid has special geometry property, it is noted the critical triangle ΔBCD is an equilateral triangle, so the relationship of the three angles are obtained as $\tan \beta = 2 \tan \alpha$, $\tan \gamma = \sqrt{3} \tan \alpha$, and the vertical distance between the apex A and the spherical cap surface is

$$AF = R_0 / \sin \beta - R_0 \tag{1}$$

Furthermore, two more critical values Δ_1 and Δ_2 are defined for the following scratching description, which are shown in Figs. 1(b) and (c), respectively.

$$\Delta_1 = R_0 - R_0 \sin^2 \alpha / \sin \beta - r_0 \cos \alpha \tag{2}$$

$$\Delta_2 = R_0 - R_0 \sin \beta \tag{3}$$

where r_0 is the radius of arc BC and $r_0 = \sqrt{R_0^2 - \left(R_0 \sin \alpha / \sin \beta \right)^2}$.

According to the spherical capped regular three side pyramidal tip model, when the scratching depth h is less than Δ_1, only part spherical cap of the probe tip participates in scratching. While in the range from Δ_1 to Δ_2, both the probe tip cap and pyramidal base will be involved in the scratching, the tip-sample interface is complicated. When the scratching depth h is larger than Δ_2, the spherical cap will completely take part in the cutting, and further the spherical cap can be ignored when the scratching depth is far larger than Δ_2. According to the above analysis, the tip model selection for different scratching depth is based on the value of Δ_2, and the Eq. (3) shows the value of Δ_2 is related with the face angle and the tip radius, the corresponding relationship is shown in Fig. 3, indicating a larger face angle and tip radius leads to a larger value of Δ_2.
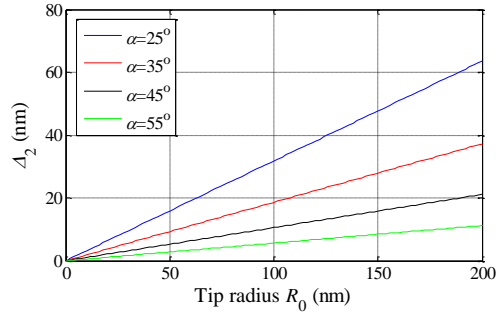

Fig. 3. Values of Δ_2 with different tip radius and face angle

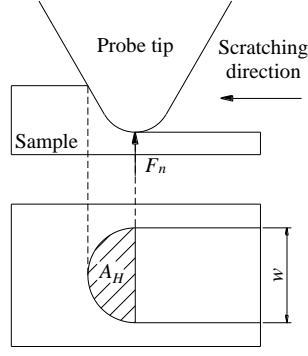## 2.2. The horizontal projected area of tip-sample interface

Fig. 4 the schematic of probe tip based scratching

As shown in Fig. 4, for general probe tip, it has been widely accepted that the normal force F_n is the product of the flow stress σ_p of the sample material and the horizontal projected area A_H of the tip-sample interface [8-12], as described in Eq. (4), where the area A_H is a function of the scratching depth h.

$$F_n = \sigma_p A_H (h) \tag{4}$$

In the scratching of the spherical capped conical tip model, only the spherical cap surface of the tip model contacts with the sample, the horizontal projected area of the tip-sample interface can be easily obtained as

$$A_H = \frac{\pi}{2} \left(\frac{w}{2} \right)^2 \tag{5}$$

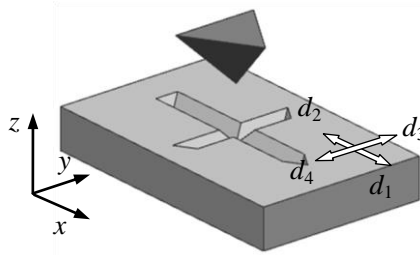where w is the width of nanochannel and defined by $w = 2\sqrt{R_0^2 - (R_0 - h)^2}$.

Fig. 5. Scratching in four different directions of pyramidal tip model

In the scratching of the spherical capped regular three side pyramidal tip model, the cutting surface is different in the four scratching directions due to the pyramid geometric characteristics, and thus leading to different tip-sample interface. As a result, it is necessary to consider the scratching direction in the calculation of the horizontal projected area of the tip-sample interface, and four mutually perpendicular scratching directions expressed by d_1-d_4 are defined as shown in Fig. 5.

The horizontal projected areas of the tip-sample interface of the regular three side pyramid tip model scratching in four directions are shown in Fig. 6, where the red dotted line is the scratched groove, the shaded area is the horizontal projected area of the tip-sample interface. In the scratching direction d_1, two pyramid surfaces contact with the sample, and they are symmetric about the cutting blade, the corresponding horizontal projected areas A_{Hd1} of the tip-sample interface and the scratching width w_{d1} are shown in Fig. 6(a). In the scratching direction d_2, as shown in Fig. 6(b), only one pyramid surface contacts with the sample and so the area A_{Hd2} is half of A_{Hd1}, but the scratching width is equal.

$$A_{Hd1} = 2\sqrt{3}\left(AF + h\right)^2 \tan^2 \alpha \tag{6}$$

$$A_{Hd2} = A_{Hd1}/2 \tag{7}$$

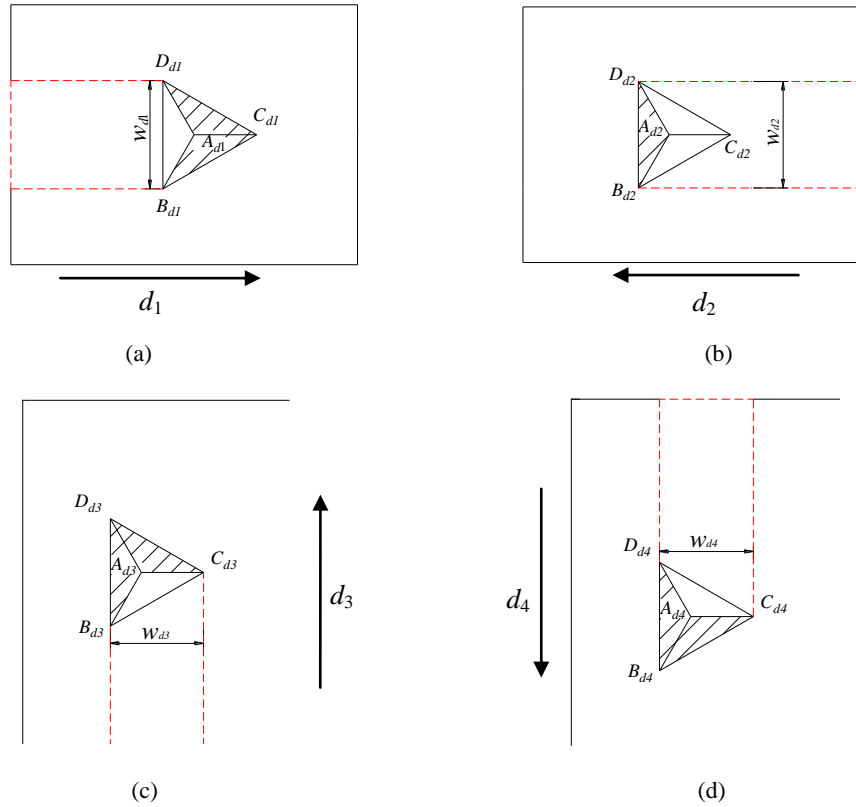$$w_{d1} = w_{d2} = 2\left(AF + h\right)\tan \gamma \tag{8}$$

Fig. 6. Horizontal projected areas of the tip-sample interface of the regular three side pyramid tip model scratching in the four directions.

In the scratching directions d_3 and d_4, the scratching process is same, two pyramid surfaces contact with the sample, but they are not symmetric about the cutting blade. According to Figs. 6(c) and (d), the horizontal projected area of tip-sample interface is equal to that in the scratching direction d_1, but the scratching width is decided by

both the face angle and edge angle.

$$A_{Hd3} = A_{Hd4} = A_{Hd1} \tag{9}$$

$$w_{d3} = w_{d4} = (AF + h)(\tan\alpha + \tan\beta) \tag{10}$$

3. SPH simulation model

3.1. SPH method

SPH is a mesh-less method based on Lagrangian method, the sample is discretized with a set of SPH particles, which include the material properties and state variables. Compared with the traditional finite element analysis, SPH method can easily deal with large distortions, because the chips can naturally separate from the sample. This kind of method has been successfully applied in the micro cutting [27-29].

3.2. Simulation model

Both spherical capped conical tip model and spherical capped regular three side pyramid model are seen as rigid in the simulation, which are constructed and meshed in ANSYS environment firstly, and then they are imported into the LS-DYNA software to implement the scratching with the SPH sample model. The scratching depth is from 20nm to 200nm in this paper.

Generally, in order to avoid the effect of the sample boundary on the simulation accuracy, a larger sample model is needed when the scratching depth is large, and thus if the particle size keeps constant, there will be too many SPH particles in the simulation of large scratching depth, which will lead to a very long simulation time. Therefore, the SPH particle diameters are changed based on the scratching depth in this paper. The boundary dimension of the sample should be large enough that the boundaries do not generate stress during the scratching, which may cause uncertainty to the simulation results, so the sample dimension changes based on the scratching depth and direction, a larger scratching depth needs a larger sample model. In the sample modeling, the particle number is reduced or keeps invariable, but the boundary dimension is increased due to the increase of SPH particle diameter. After many attempts, the diameter and the number of SPH particle for different scratching depth are listed in Table 1.

The sketch of the scratching model is shown in Fig. 7. The bottom surface of the sample is fixed in the whole six degrees of freedom, the translational motion of the front and back boundary surfaces along the scratching direction are constrained, and the translational motion of bilateral boundary surfaces are constrained in the horizontal vertical direction of the scratching direction. The SPH scratching model of spherical capped conical tip

and the spherical capped regular three side pyramidal tip are shown in Figs. 8 (a) and (b), respectively.

Table 1 SPH particle diameter in different scratching depth

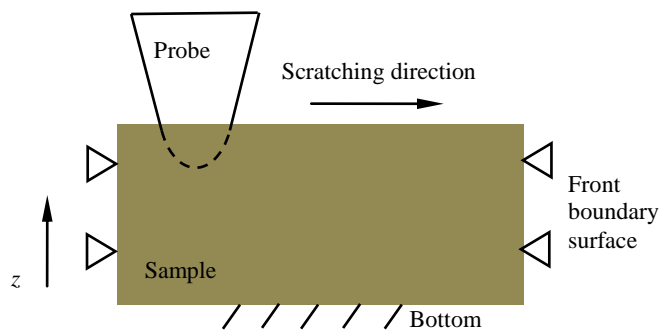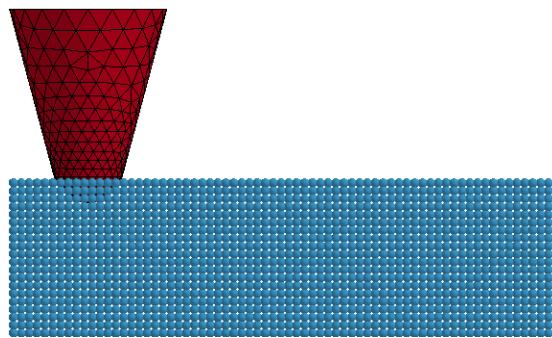|	Sample model for spherical capped conical tip scratching			Sample model for spherical capped regular three side pyramidal tip scratching			
Scratching depth (nm)	20	40	60	80	120	160	200
SPH particle diameter (nm)	7	14	20	20	30	40	50
SPH particle number (scratching direction ×lateral direction ×z direction)	90×90×30	90×60×30	75×50×25	75×50×25	75×50×25	60×50×25	60×50×25

Fig. 7. Sketch of the scratching model

(a) SPH simulation model of spherical capped conical tip
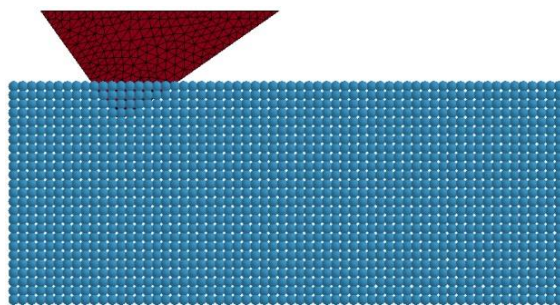
(b) SPH simulation model of spherical capped regular three side pyramidal tip

Fig. 8. The SPH simulation model

The probe tip is seen as rigid with density 3520kg/m^3, young's modules 1100Gpa and poison's ratio 0.29. The Oxygen-Free High-Conductivity (OFHC) cooper is selected as sample and described by Johson-Cook model [30], which has been widely used in engineering for the simple form and few parameters. It can be expressed in the following form.

$$\sigma = \left(A + B\varepsilon^n \right)\left(1 + C\ln\frac{\dot{\varepsilon}}{\dot{\varepsilon}_0} \right)\left[1 - \left(\frac{T - T_0}{T_m - T_0} \right)^m \right] \tag{11}$$

where σ is the equivalent stress, ε is the equivalent plastic strain, $\dot{\varepsilon}$ and $\dot{\varepsilon}_0$ are the current and reference strain rates respectively, T_m is the melting temperature, T is the experimental temperature, and T_0 is the room temperature. A B n C and m are unknown parameters, which can be obtained from the experimental testing, and the corresponding values used in this paper are listed in Table 2 [27, 28, 31].

Table 2 Parameters of the Johson-Cook model of OFHC cooper

Density (ρ)	8900kg/m^3
Young's modules (E)	110Gpa
Poisson's ratio (v)	0.32
A	0.09
B	0.292
n	0.31
C	0.025
m	1.09
Melting temperature (T_m)	1356K
Room temperature (T_0)	293K
Specific heat	383J/(kg·K)
Spall stress (σ)	1.95Gpa

4. Simulation and discussion

4.1. The effect of scratching speed

Considering the wide applications of spherical capped conical tip model, this model is selected for the analysis of the effect of scratching speed on the scratching process. Three scratching speeds of 10μm/μs, 1μm/μs and 0.1μm/μs are simulated under a scratching depth 60nm on the same sample model. The simulation results including normal force and cutting force along the scratching direction are shown in Fig. 9. Although the speed is far higher

than the actual scratching speed, the approximate trend is acceptable. According to the simulation results, both the normal force and cutting force increase a little with the increase of the scratching speed, the reasonable explanation is that the generated chips cannot flow away in time in high scratching speed, leading to the area increase of tip-sample interface. It is noted the increase of the normal force is very limited, therefore, in order to save simulation time the scratching speed in following simulation adopts 10μm/μs.

The friction coefficient is another effective parameter to assess the scratching process, which is defined as the ratio of the cutting force and the normal force [19, 32]. According to Fig. 9 (a) and (b), the friction coefficient with scratching speed 10μm/μs, 1μm/μs and 0.1μm/μs in stable scratching state is 0.82, 0.87 and 0.91, respectively. The friction coefficient is reduced with the increase of the scratching speed, the possible reason is the probe tip with faster scratching speed has larger kinetic energy, the generated chips are easier to crack in front of the tip, so the cutting force increases less than the normal force.
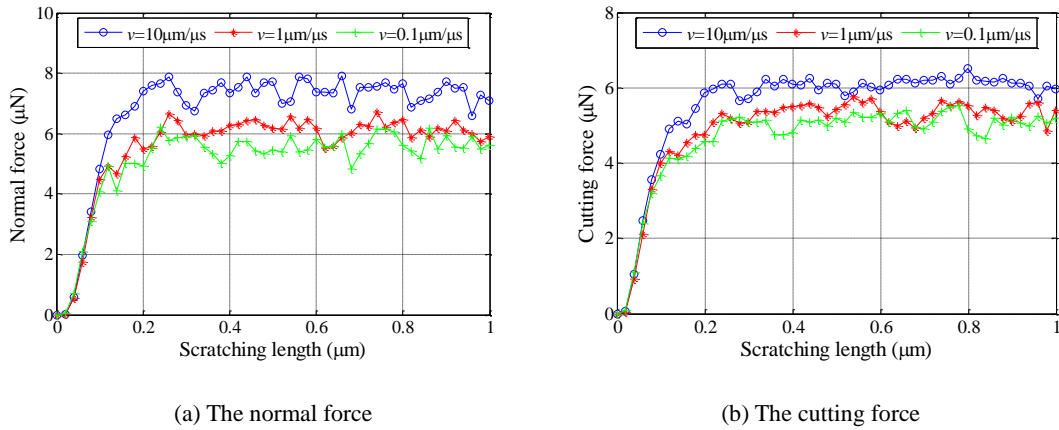

| (a) The normal force | (b) The cutting force |

Fig. 9. The normal force and lateral force of spherical capped conical tip model with different scratching speed

4.2. The effect of scratching depth and scratching direction

According to the analyses in section 2, the spherical capped conical tip model is used in the scratching depth smaller than 60nm, and the spherical capped regular three side pyramidal tip model is used in the scratching depth larger than 60nm. Three scratching depths of 20nm, 40nm and 60nm are selected for the spherical capped conical tip model scratching simulation. In order to save the simulation time, the scratching length is 0.3μm in depth of 20nm, and 1μm in depth of 40nm and 60nm. The normal forces generated during the scratching with the three scratching depths are shown in Fig. 10.

The spherical capped regular three side pyramidal tip model with $\alpha=35^{o}$ are firstly selected for the scratching simulation. According to Eq. 3, the value of Δ_2 is about 16nm, based on the analysis in section 2, the area function of three side pyramid tip model is more applicable when the scratching depth is far larger then Δ_2, so the scratching

depths of 80nm, 120nm, 160nm and 200nm are selected. The normal force of the spherical capped regular three side pyramidal tip model is related with the scratching direction, so the simulations are processed in all four directions, the generated normal forces in different scratching depth are shown in Fig. 11, and the scratched grooves in scratching depth of 160nm are shown in Fig. 12.
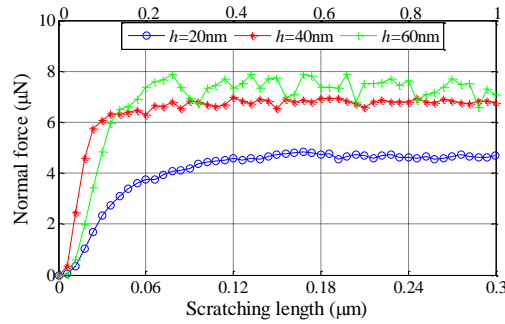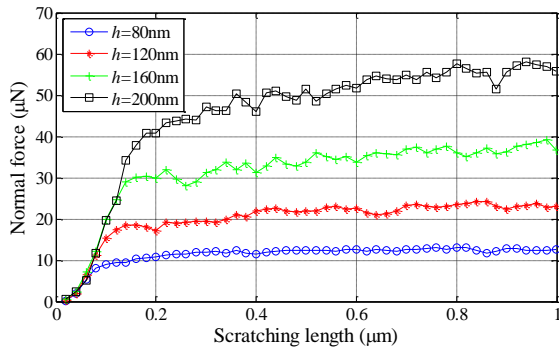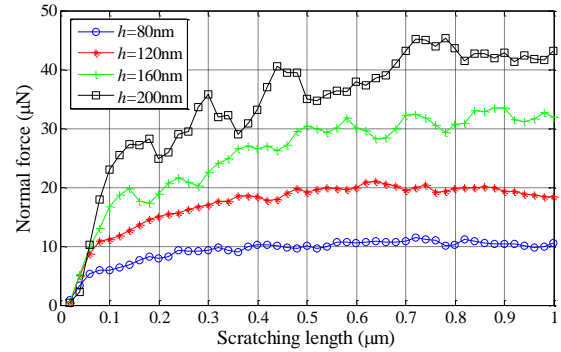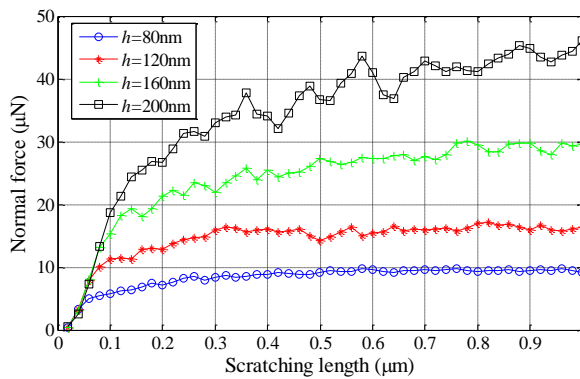

Fig. 10. The normal force of spherical capped conical tip model with different scratching depth

(a) d_1 direction

(b) d_2 direction

(c) d_3 and d_4 direction

Fig. 11. The normal force of spherical capped regular three side pyramidal tip model with different scratching depth.

(a) d_1 direction

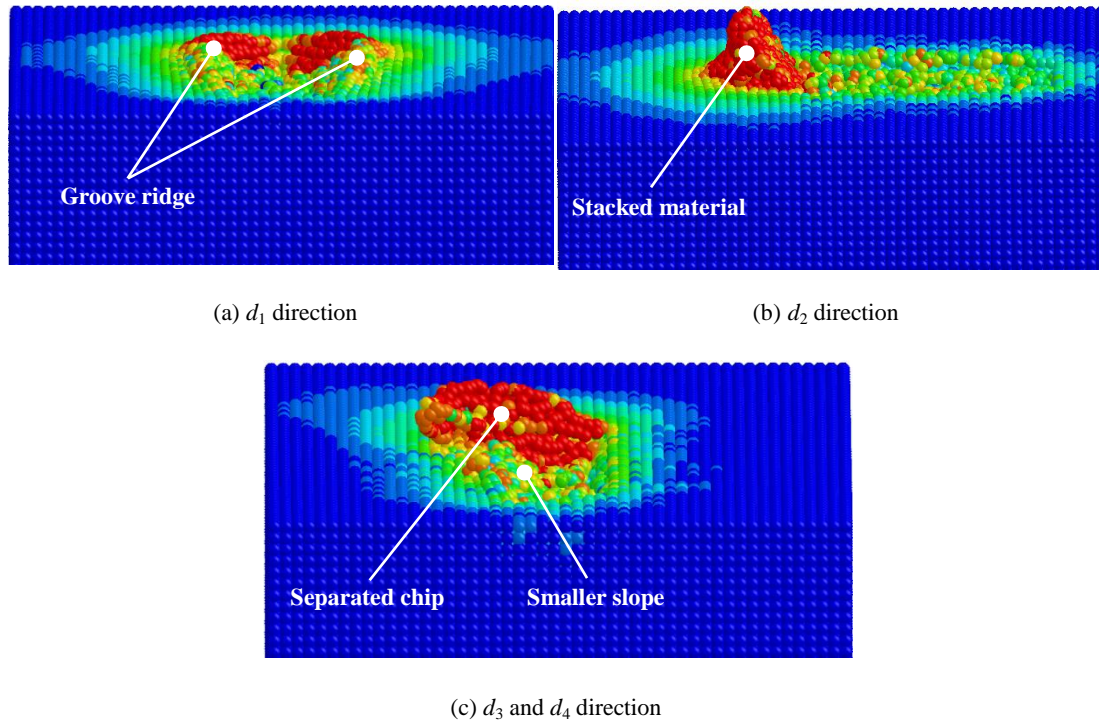(b) d_2 direction

(c) d_3 and d_4 direction

Fig. 12. The chips generated by spherical capped regular three side pyramidal tip model in different direction

In both Figs. 10 and 11, the normal forces increase with the increase of scratching depth and reach a steady value after a period of time, which means the scratching goes into steady state. The larger of the scratching depth, the slower to the steady scratching state, this is because more materials deform in the large scratching depth, which need more time to transfer the deformation. Comparing the normal force of Figs. 11(a) and (c), it is noted that the normal force in the d_1 direction is larger than that in the d_3 direction, but they should be equal according to the theoretical analysis. This is because in the d_1 direction, most removed material are divided into two sides of the groove and form ridge due to the cut of front blade of the pyramid, as shown in Fig. 12(a), which leads to the increase of the tip-sample interface in some degree, and further a larger normal force; while in the d_3 and d_4 directions, the removed material flow to the side of the groove with smaller slope, as shown in Fig. 12(c), the separated chips are easy to form than that in the d_1 direction, although the chips also contact with the probe tip, but the force will be very small. In the d_2 direction, the normal force is extremely larger than half of the normal force in the d_1 and d_3 directions, which is because the removed material can only flow away along the front pyramid surface, resulting in a mess of stack of the material, as shown in Fig. 12(b), this will increase the tip-sample interface significantly.
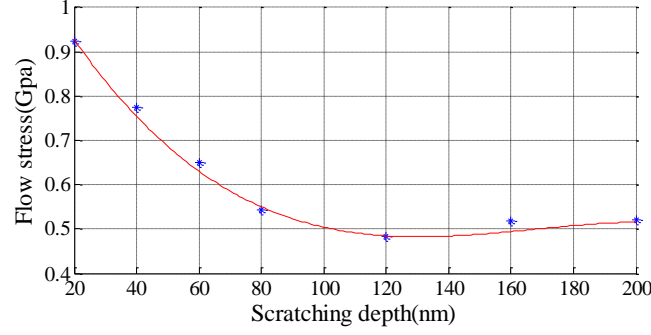
Fig. 13. The flow stress of the sample (OFHC cooper)

Based on the generated normal force of the spherical capped conical tip and spherical capped regular three side pyramidal tip in the d_3 and d_4 directions, the flow stress of the sample is obtained in scratching depth from 20nm to 200nm, which is shown in Fig. 13. This indicates that the flow stress is high in small depth, and then reduces to a steady value of 0.5Gpa with the increase of the scratching depth. A cubic function is used to fit the discrete flow stress point, and it can be expressed by following equation.

$$stress = -1.65 \times 10^{-7} h^3 + 8.29 \times 10^{-5} h^2 - 1.32 \times 10^{-2} h + 1.16 \qquad (12)$$
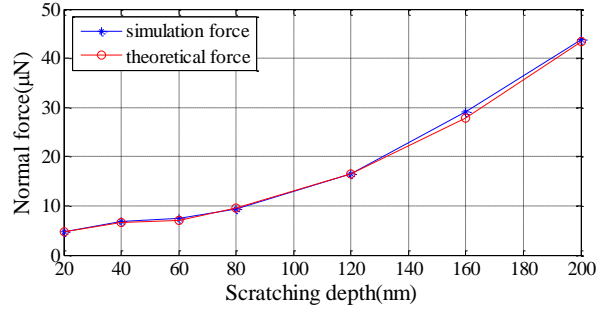
Based on Eq. (12), the comparison of the theoretical and simulation normal force is shown in Fig. 14. In the scratching depth from 20nm to 60nm, the normal forces agree very well for the spherical capped conical tip model. In the scratching depth from 80nm to 200nm, the compliance degree depends on the scratching direction. Due to the groove ridge in the d_1 direction and the material stack in the d_2 direction, the simulated normal force is relatively larger than that of the theoretical calculation, the error is about 25% in the d_1 direction, but in the d_2 direction the simulated force is almost twice of that of the theoretical force. In the d_3 direction, the simulated normal forces are in agreement with those of the theoretical calculation.
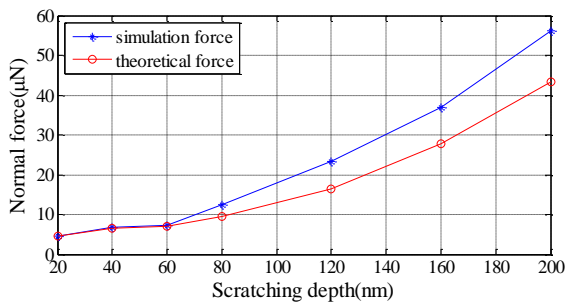
(a) d_1 direction
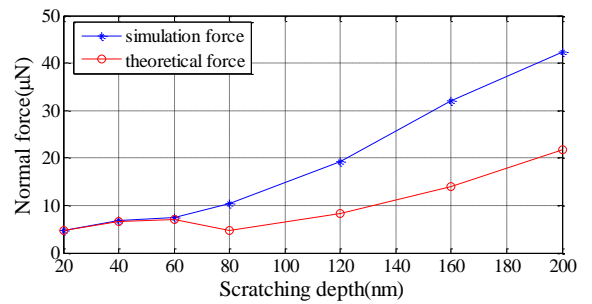
(b) d_2 direction

(c) d_3 direction

Fig. 14. The comparison of the normal force in simulation and theoretical calculation in different scratching direction

4.3. The effect of the face angle

In the spherical capped regular three side pyramidal tip scratching, the face angle has significant influence on the tip-sample interface area, and thus a series of simulation with different face angle (25˚, 35˚, 45˚, 55˚) are conducted in this paper. According to previous analyses, the simulated normal force in the d_3 and d_4 directions are in good agreement with those of the theoretical calculation, so the simulation is performed in the d_3 direction with scratching depth 160nm. The simulation results of the generated chips and the von mises stress are shown in Fig. 15, which indicates the separated chips are formed in small face angle of 25˚ and 35˚, but when the face angle reaches up to 45˚or larger, the separated chips cannot break away from the sample and even be replaced by ridge on left side of the groove, where the slope is smaller than that on the right side. Moreover, the pyramidal model with bigger face angle results in larger groove width and residual stress area during the scratching. These phenomena are explained as follows.

According to Fig. 6(c) and (d), one of the two contacted surface in the d_3 direction is parallel with the scratching direction, the other is called the material flow surface, where the chips flow away from this surface. Considering the cutting blade and the material flow surface are in three dimensional space relative to the scratching direction, the material flow direction is divided in horizontal plane and C-C plane as shown in Fig. 16. In the horizontal plane, the material flow along the edge of the probe cross section, the flow angle is 60 ° relative to the scratching direction, which is same for all regular three side pyramidal probe tip; In the C-C plane, the flow direction is upward along the material flow surface and the flow angle is approximately equal to the face angle α. Thus, with the increase of the face angle, the material flow direction in C-C plane becomes more parallel to the horizontal plane, the material flow space between the material flow surface and the sample surface becomes smaller, which slow down the material flow speed and make the removed material difficult to separate from the sample, leading to the phenomenon of groove ridge and larger residual stress area.

The simulated normal forces during the scratching are compared with the theoretical normal forces, and the results are shown in Fig. 17. It is noted that the normal forces are in good agreement in small face angles of 25˚ and 35˚, but the errors reach up to 36.5% and 47.5% in face angles of 45˚ and 55˚, respectively. This is because the removed material flow away in small face angles of the 25˚ and 35˚, but form the groove ridge in larger face angle of 45˚ and 55˚, and the phenomenon has increased trend with the increase of face angle, the groove ridge usually leads to a larger tip-sample contact area and normal force, further a larger error.
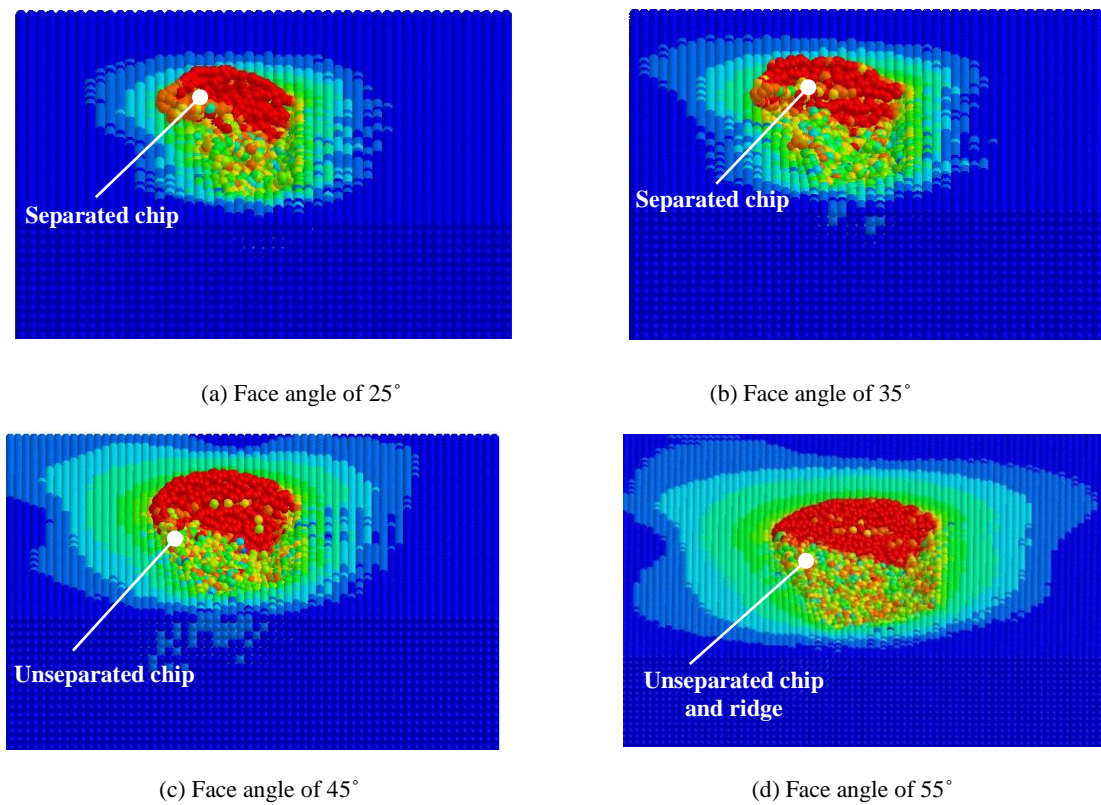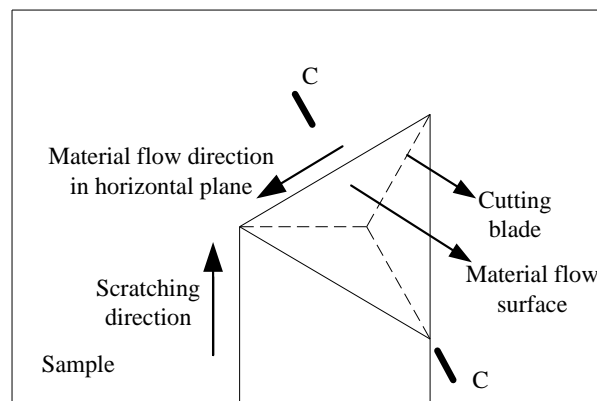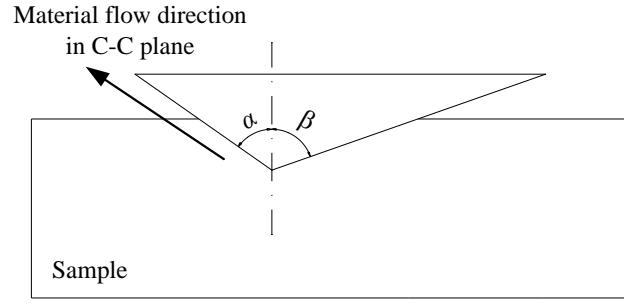

(a) Face angle of 25˚

(b) Face angle of 35˚

(c) Face angle of 45˚

(d) Face angle of 55˚

Fig. 15. The scratching process of spherical capped regular three side pyramidal tip model with different face angle

(a) In horizontal plane

(b) In C-C plane

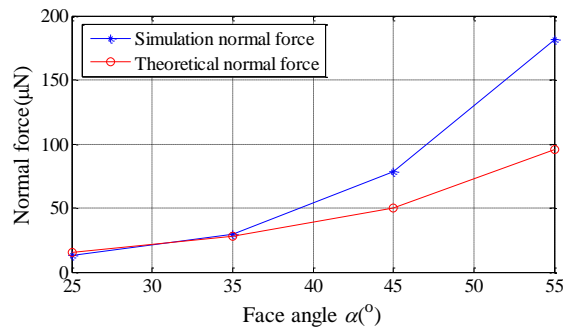Fig. 16. The material flow direction

Fig. 17. The normal force of the spherical capped regular three side pyramidal tip model with different face angle

5. Conclusions

A spherical capped conical tip model and a spherical capped regular three side pyramidal tip model are introduced for the common three side probe tip. The former is used in the small scratching depth from 20nm to 60nm and the latter is used in the larger scratching depth from 80nm to 200nm. The horizontal projected areas of the tip-sample interface of these two models during the scratching are theoretically analyzed for the calculation of the normal force. In the scratching simulation, the probe tips are seen as rigid, and the sample is constructed with Johnson-Cook model. The SPH method is adopted for the simulation in LS-DYNA software.

According to the simulation results, a higher scratching speed leads to a larger normal force and cutting force, but the increase is limited, the normal force increases with the increase of scratching depth in both models. In the scratching simulation of spherical capped regular three side pyramidal tip model, the scratching process is different in different directions. In the d_1 direction, due to the cut of front blade of the pyramid model, most of the removed materials are divided to two sides of groove and form ridge; in the d_2 direction, a lot of removed materials stack in the front pyramid surface; in the d_3 and d_4 directions, the removed materials flow to the side with smaller slope of the groove, and it is easier to form separated chips than in d_1 direction. In conclusion, the normal forces scratched in the d_3 and d_4 direction are closest to the theoretical calculation. Furthermore, the increase of face angle leads to

the increase of the normal force and the residual stress area, and the error between the theoretical and simulated normal forces is also getting large when the face angle is bigger than 35˚.

References

[1] J. L. Perry, S. G. Satish, "Review of fabrication of nanochannels for single phase liquid flow", Microfluidics and Nanofluidics, vol. 2, no. 3, pp. 185–193, 2006.

[2] Y. Yan, T. Sun, Y. Liang, S. Dong, "Investigation on AFM-based micro/nano-CNC machining system", International Journal of Machine Tools & Manufacture, vol. 47, pp.1651–1659, 2007.

[3] B. A. Gozen, O. B. Ozdoganlar, "Design and evaluation of a mechanical nano manufacturing system for nano milling", Precision Engineering, vol.36, pp. 19-30, 2012.

[4] K. Bourne, S. G. Kapoor, R. E. DeVor, "Study of a High Performance AFM Probe-Based Microscribing Process", Journal of Manufacturing Science and Engineering, Vol. 132, p. 030906, 2010.

[5] W. P. Jeong, C. C. Soo, C. Hyun, "Portable nano probe for micro/nano mechanical scratching and measuring", Transaction of Nonferrous Metals Society of China, vol. 21, pp. s205-s209, 2011.

[6] Y. Geng, Y. Yan, X. Zhao, "Fabrication of millimeter scale nanochannels using the AFM tip-based nanomachining method", Applied Surface Science, vol. 266, pp. 386-394, 2013.

[7] G. Gu, L. Zhu, C. Su, H. Ding and S. Fatikow, "Modeling and control of piezo-actuated nanopositioning stages: A survey," IEEE Transactions on Automation Science and Engineering, vol. 13, no. 1, pp. 313-332, 2016.

[8] Z. Lin, Y. Hsu, "A study of estimating cutting depth for multi-pass nanoscale cutting by using atomic force microscopy", Wear, vol. 258, pp. 4513-1522, 2012.

[9] Z. Wang, N. Jiao, S. Tung, Z. Dong, "Research on the atomic force microscopy-based fabrication of nanochannels on silicon oxide surfaces", Chinese science bulletin, vol. 55, no. 30, pp. 3466-3471, 2010.

[10] Z. Wang, N. Jiao, S. Tung, Z. Dong, "Atomic force microscopy-based repeated machining theory for nanochannels on silicon oxide surfaces", Applied Surface Science, vol. 257, pp. 3627-3631, 2011.

[11] Z. Wang, N. Jiao, S. Tung, Z. Dong, "Material removal model for AFM-based nanochannel fabrication",

Wear, vol. 278, pp. 71-76, 2012.

[12] Y. Geng, Y. Yan, Y. Xing, "Modelling and experimental study of machined depth in AFM-based milling of nanochannels", International Journal of Machine Tools & Manufacture, vol. 73, pp. 87–96, 2013.

[13] Y. Geng, Y. Yan, Y. Xing, Q. Zhang, X. Zhao, and Z. Hu, "Effect of cantilever deformation and tip-sample contact area on AFM nanoscratching", Journal of vacuum science & technology B, vol. 31, p. 061802, 2013.

[14] B. Meng, F. Zhang, Z. Li, "Deformation and removal characteristics in nanoscratching of 6H-SiC with Berkovich indenter", Materials Science in Semiconductor Processing, vol. 31, pp. 160-165, 2015.

[15] C. Pan, T. Wu, C. Liu, et al, "Study of scratching Mg-based BMG using nanoindenter with Berkovich probe", Materials Science and Engineering A, vol. 527, pp. 2342-2349, 2010.

[16] B. Meng, Y. Zhang, F. Zhang, "Material removal mechanism of 6H-SiC studied by nano-scratching with Berkovich indenter", Applied Physics A, vol. 122, p. 247, 2016.

[17] P. Zhu, Y. Hu, T. Ma, H. Wang, "Study of AFM-based nanometric cutting process using molecular dynamics", Applied Surface Science, vol. 256, pp. 7160–7165, 2010.

[18] Q. Pei, C. Lu, H. Lee, "Large scale molecular dynamics study of nanometric machining of copper", Computational Materials Science, vol. 41, pp. 177–185, 2007.

[19] J. Zhang, T. Sun, Y. Yan, Y. Liang, "Molecular dynamics study of scratching velocity dependency in AFM-based nanometric scratching process", Materials Science and Engineering A, vol. 505, pp. 65-69, 2009.

[20] J. Zhang, T. Sun, Y. Yan, et al, "Molecular dynamics simulation of subsurface deformed layers in AFM-based nanometric cutting process", Applied Surface Science, vol. 254, pp. 4774-4779, 2008.

[21] Y. Yan, T. Sun, S. Dong, Y. Liang, "Study on effects of the feed on AFM-based nano-scratching process using MD simulation", Computational Materials Science, vol. 40, pp. 1-5, 2007.

[22] P. Zhang, H. Zhao, C. Shi, et al, "Influence of double-tip scratch and single-tip scratch on nano-scratching process via molecular dynamics simulation", Applied Surface Science, vol. 280, pp. 751-756, 2013.

[23] T. Fang, C. Liu, S. Shen, et al, "Nanoscratch behavior of multi-layered films using molecular dynamics", Applied Physics A, vol. 90, pp. 753-758, 2008.

[24] R. Gingold and J. Monaghan, "Smoothed particle hydrodynamics: theory and application to non-spherical stars," Monthly Notices of the Royal Astronomical Society, vol. 181, pp. 375-89, 1977.

[25] A. Vázquez-Quesada, M. Ellero, "Rheology and microstructure of non-colloidal suspensions under shearstudied with Smoothed Particle Hydrodynamics", Journal of Non-Newtonian Fluid Mechanics, vol. 233, pp. 37-47, 2016.

[26] W. Li, S, Yin, X. Wang, Numerical investigations of the effect of oblique impact on particle deformation in cold spraying by the SPH method, Applied Surface Science, vol. 256, pp. 3725-3734, 2010.

[27] H. Zhao, P. Zhang, H. Liu, "Influences of residual stress induced by cutting on subsequent scratch using smooth particle hydrodynamic (SPH)", Materials Transactions, vol. 55, pp. 1440-1444, 2014.

[28] H. Zhao, C. Liu, T. Cui, et al, "Influences of sequential cuts on micro-cutting process studied by smooth particle hydrodynamic", Applied Surface Science, vol. 284, pp. 366-371, 2013.

[29] J. Cao, Y. Wu, J. Li, Q. Zhang, "Study on the material removal process in ultrasonic-assisted grinding of SiC ceramics using smooth particle hydrodynamic (SPH) method", International Journal of Advanced Manufacturing Technology, vol. 83, pp. 985-994, 2016.

[30] G. R. Johnson, W. H. Cook, "A constructive model and data for metals subjected to large strains, high strain rates and high temperatures", in: Proceedings of the Seventh International Symposium on Ballistics, pp. 541-547. 1983.

[31] L. Campagne, L. Daridon and S. Ahzi, "A physically based model for dynamic failure in ductile metals", Mechanics of Materials, vol. 37, pp. 869-886, 2005.

[32] M. Malekian, S. Park, D. Strathearn1, M. G. Mostofa1 and M. Jun, "Atomic force microscope probe-based nanometric scribing", Journal of Micromechanics and Microengineering, vol. 20, p. 115016 2010.